

RCM-Fusion: Radar-Camera Multi-Level Fusion for 3D Object Detection

Jisong Kim^{*1} Minjae Seong^{*1} Geonho Bang¹ Dongsuk Kum² Jun Won Choi^{†1}
¹Hanyang University ²KAIST

{jskim, mjseong, ghsbang}@spa.hanyang.ac.kr, dskum@kaist.ac.kr, junwchoi@hanyang.ac.kr

Abstract

While LiDAR sensors have been successfully applied to 3D object detection, the affordability of radar and camera sensors has led to a growing interest in fusing radars and cameras for 3D object detection. However, previous radar-camera fusion models have not been able to fully utilize radar information in that initial 3D proposals were generated based on the camera features only and the instance-level fusion is subsequently conducted. In this paper, we propose radar-camera multi-level fusion (RCM-Fusion), which fuses radar and camera modalities at both the feature-level and instance-level to fully utilize radar information. At the feature-level, we propose a Radar Guided BEV Encoder which utilizes radar Bird's-Eye-View (BEV) features to transform image features into precise BEV representations and then adaptively combines the radar and camera BEV features. At the instance-level, we propose a Radar Grid Point Refinement module that reduces localization error by considering the characteristics of the radar point clouds. The experiments conducted on the public nuScenes dataset demonstrate that our proposed RCM-Fusion offers 11.8% performance gain in nuScenes detection score (NDS) over the camera-only baseline model and achieves state-of-the-art performances among radar-camera fusion methods in the nuScenes 3D object detection benchmark. Code will be made publicly available.

1. Introduction

Accurate perception of the surrounding environments is crucial for successfully implementing self-driving robots or vehicles. Over the last decade, research into 3D object detection has focused on leveraging LiDAR data which offers precise spatial information, and camera data which provides rich semantic information. However, LiDAR sensors may render them impractical due to their high cost, so radar sensors are emerging as a low-cost alternative. Radar sensors use radio waves to detect, locate and track

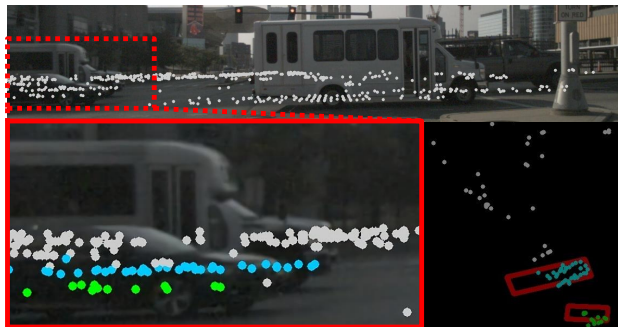


Figure 1. Illustration of radar points projected to a camera view. Due to the multi-path propagation nature of radars, there can be situations where points are taken in visually obscured areas. If you look at the zoom-in image, the points inside the sedan all appear to be reflecting off the sedan. However, when examining the points on the BEV, it is evident that some of them reflect from the white van behind the sedan or other objects behind the van.

objects in their vicinity. Radar sensors furnish both the 3D location of an object and its attributes, including Radar Cross Section (RCS) and Doppler velocity information. The 77GHz radars used for automotive applications have a higher wavelength than the LiDAR, making them more reliable in adverse weather conditions. Utilizing the advantages of these radar sensors, the previous literature has demonstrated that radar-camera fusion models can yield performance comparable to LiDAR-based 3D object detectors [4, 12, 26, 27, 30, 31, 38, 42, 43, 44, 47, 48].

Recent studies have proposed several radar-camera fusion models that significantly improved 3D object detection performance, providing depth and velocity [11, 20, 24]. The existing methods in [11, 20, 24] produce 3D box proposals from the camera image and associate the radar data represented in point clouds with 3D proposals in a camera-view to refine the initial results. Nevertheless, these instance-level fusion methods have two limitations. First, the performance of the instance-level fusion relies on the quality of 3D proposals obtained from the camera-based object detectors. Radar is not leveraged during the initial proposal generation process, thus not exploiting its full potential. Second, the fusion of camera and radar data is performed from

^{*}Equal contribution.

[†]Corresponding author.

a camera view, which makes it challenging to establish the correct associations between the data acquired by the two sensors. The point clouds obtained from radar sensors may have inaccurate height measurements due to a lack of vertical resolution, which means that when radar points are projected into the camera view, the correspondence between projected radar points and image pixels is not precise. Fig. 1 shows radar points projected onto a camera image where one object is occluded by another. Due to inaccurate height measurements, some of radar points lying on the front object in the camera view correspond to those reflecting from other objects behind. Such radar characteristics can lead to significant association errors between radar and camera data and limit the potential benefits of sensor fusion.

The aforementioned issues motivate us to attempt radar-camera feature fusion in the bird’s eye view (BEV) domain. BEV representation is robust to inaccurate height data from radar points, making radar-camera association more robust. The key to successful fusion in the BEV domain is appropriately accounting for the geometric relationship between the camera and radar features to transform them into precise BEV representations. Generating an accurate BEV feature map is still challenging due to the high uncertainty in the depth information from the camera. The position information from the radar sensors can be used to guide the camera features to accurately translate from camera view to BEV.

In this paper, we propose a multi-level fusion architecture for 3D object detection, referred to as *Radar-Camera Multi-level Fusion (RCM-Fusion)*. The proposed method achieves the fusion of radar and camera features at two different levels. RCM-Fusion first attempts feature-level fusion to produce a dense BEV feature map with which 3D proposals are generated. Then, it performs the instance-level fusion to refine the proposals through a grid point-based proposal feature fusion.

For feature-level fusion, we devise Radar Guided BEV Query, which utilizes the positional information of radar to transform the image features into distinct BEV features. Then, we employ the Radar-Camera Gating module to obtain the weighted aggregation of multi-modal BEV feature maps. Such an adaptive feature aggregation module is integrated into transformer layers, which successively decode the dense BEV query features. For instance-level fusion, we propose the Proposal-aware Radar Attention module to obtain radar point features that take into consideration their relevance to the 3D proposal. Then, we employ a novel adaptive grid point pooling method, Radar Grid Point Pooling, which accounts for the positional uncertainty of radar points for instance-level fusion. Finally, to improve the efficacy of radar data utilization and obtain high-quality radar points for RCM-Fusion, we modified the basic radar data filtering and multi-sweep methods used in the nuScenes dataset [1]. As a result, our model significantly outper-

formed camera-only baseline models and achieved state-of-the-art performance among the radar-camera fusion methods on the nuScenes 3D object detection benchmark [1].

The key contributions of our work are as follows:

- We present a state-of-the-art radar-camera fusion method for 3D object detection. The proposed RCM-Fusion combines radar and camera features at both the feature-level and instance-level. This is in contrast to the existing radar-camera fusion methods [11, 20, 24], which perform instance-level fusion only.
- We propose a **feature-level fusion** which transforms the image features into accurate BEV features through Radar Guided BEV Query and adaptively fuses multi-modal BEV features via Radar-Camera Gating modules. This feature-level fusion generates a dense BEV feature map, which is used to produce the initial 3D proposals.
- We propose an **instance-level fusion** that employs Proposal-aware Radar Attention to reduce the impact of irrelevant points and generates features which refine the initial results through Radar Grid Point Pooling.
- RCM-Fusion achieves an **8.4%** improvement in mean average precision (mAP) and **11.8%** improvement in the nuScenes detection score (NDS) over the camera-based baseline, recording a state-of-the-art performance of **49.3%** mAP and **58.0%** NDS on the nuScenes test set.

2. Related Work

2.1. 3D Object Detection with Multi-Camera

The challenge of 3D object detection lies in accurately representing the positions of objects in a 3D coordinate, which can be difficult when relying solely on image data [3, 6, 7, 13, 16, 19, 22, 25, 33, 34, 35, 36, 40, 45]. In early multi-camera 3D detectors [34, 45], 3D object detection was performed by incorporating a 3D regression branch based on 2D bounding box prediction. Later papers [25, 33] emphasized the importance of depth prediction in image views and proposed methods using geometric relation graphs or depth pre-training. Nevertheless, these approaches are sub-optimal since they individually address the 3D object detection problem for each image without considering the connection between various camera perspectives. Afterward, methods have been proposed to detect objects by considering the correlation between multi-camera, which can be divided into two main approaches: DETR-based and BEV-based. DETR-based methods [3, 19, 36], which use the concept of learnable object queries, extract multi-camera features from sparse 3D object queries. BEV-based methods [6, 7, 9, 13, 16, 22, 37, 40], which have

recently shown successful performance, detect objects by converting image features composed of camera views into a single BEV representation. In [6, 7], a view transformation model was used to effectively convert multi-camera feature maps to BEV representations. BEVDepth [13] emphasizes the importance of accurate depth prediction and addresses this by providing explicit depth supervision. In [9, 16, 40], an adaptive approach was proposed for converting camera-view features into BEV features by leveraging the transformer’s attention mechanism.

2.2. Radar data for 3D Object Detection

Radar-based object detection research typically focuses on the fusion of multiple sensors rather than on a single sensor. Radar-LiDAR fusion models combined the benefits of radar, such as providing radial velocity information and being unaffected by adverse weather conditions that LiDAR sensors may not be able to handle. RadarNet [39] proposed a multi-level fusion approach to enhance the accuracy of distant objects and reduce velocity errors. MVDNet and ST-MVDNet [14, 28] have demonstrated that radar data can produce more reliable results than other lidar-based models in adverse weather conditions.

Radar-camera fusion models has been conducted in order to leverage radar positional information to supplement the camera’s limited depth information. The key concept of these models was how to effectively combine data from multiple perspectives. In [17], Inverse Projection Mapping (IPM) is leveraged to convert camera data into a BEV and fuse it with radar features. GriFNet [10] utilizes 3D anchors and 3D proposals to effectively extract features from radar and camera data. CramNet [8], meanwhile, leverages a 2D segmentation model to define the foreground section of both features and then fuses them in a unified 3D environment. CenterFusion [24], CRAFT [11] reduce localization and velocity errors by employing radar information based on camera-based 3D object detection results. RADIAN [20] designed a network to estimate the positional offset between the radar returns and the object center in order to address the radar-camera association problem.

2.3. Two-stage 3D Object Detection

Two-stage 3D object detectors [4, 15, 23, 29, 30, 31, 41] have been actively developed to improve performance in models using LiDAR data. These models refine the initial prediction results by exploiting the LiDAR point cloud within the proposal boxes. Depending on how features are extracted from the points within the proposal, two-stage models can be divided into two approaches. The first approach, [15, 29, 31], certain points related to each proposal are identified as key points and PointNet++ [27] module is used to generate features based on these key points. Graph R-CNN [41] proposes a method that takes into account the

distribution of points within each proposal when identifying keypoints. For the second approach, [4, 23, 30] define a virtual set of points referred to as grid points and extract point features based on these grid points to refine initial results. PV-RCNN [30] and Voxel R-CNN [4] set $6 \times 6 \times 6$ uniformly spaced grid points for each proposal and generate point features based on them. Pyramid R-CNN [23] proposed a method that can reliably refine even when the internal points in proposals are sparse and irregularly distributed. By examining the existing approaches, we determined that considering the distribution of the point clouds associated with the initial proposal was a crucial component of the two-stage method. As a result, we implemented a grid point approach, which is more flexible than existing two-stage radar-camera detectors [11, 24, 39], to effectively generate key points according to the distribution of radar points.

3. Method

We propose a multi-level fusion approach to efficiently fuse radar point clouds and surrounding images. Fig. 2 illustrates the overall architecture of the proposed method. Initially, radar and camera data are passed through separate backbone networks to generate feature maps for each sensor. The Radar-Guided BEV Encoder module then efficiently converts the image features from the camera view to BEV and fuses them with the radar BEV features. Then, initial 3D proposals are obtained from the fused BEV feature maps using the transformer-based detection head. Finally, the Radar Grid Point Refinement module is used to refine the initial results to maximize the utilization of the radar data and improve object detection accuracy.

In Section 3.1, we outline the backbone network for both radars and cameras. In Section 3.2, we describe the details of Radar Guided BEV Encoder module, a feature-level fusion of radar and camera data. Section 3.3 presents the Radar Grid Point Refinement module, a novel instance-level fusion approach. Finally, Section 3.4 outlines the radar pre-processing techniques used to maximize the quality of the radar data in the radar-camera fusion process.

3.1. Radar and Camera Backbones

Prior to the unification of the two features on the BEV, feature extraction is conducted utilizing two separate backbone networks for radar and camera modalities. Multi-scale image features F_C are generated from each of multi-view camera images using ResNet-101 [5] with FPN [18], which are commonly employed in existing camera-based 3D object detection models. For radar data, PointPillars [12] model is used to obtain the radar feature map in BEV domain. Due to large uncertainty of height information in radar point clouds, the pillar encoding method without binning in the z dimension is an appropriate approach. The

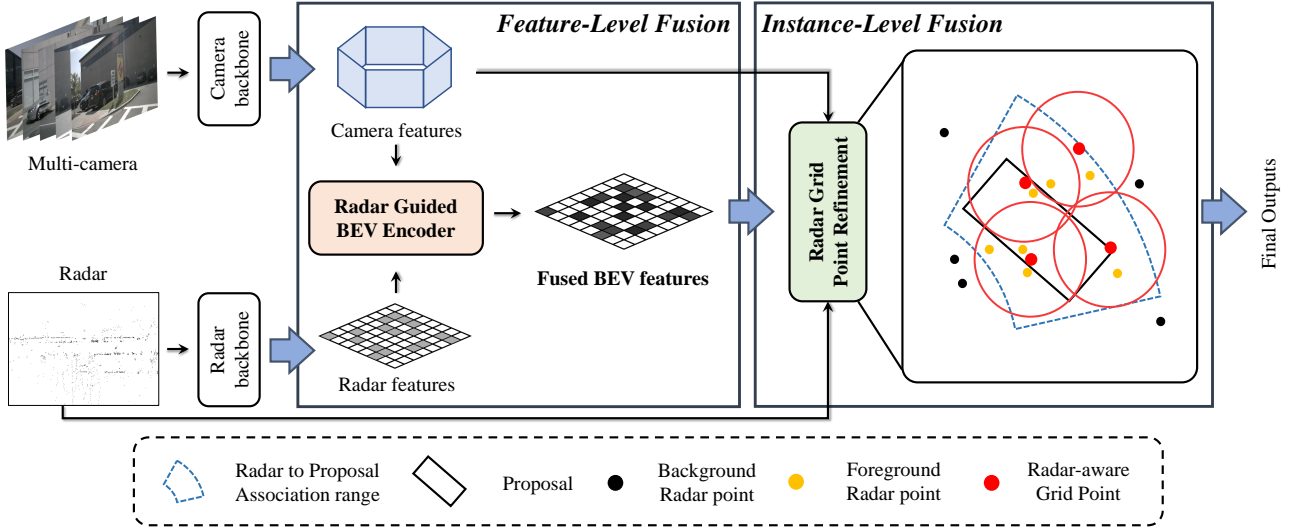


Figure 2. Overall architecture of the proposed RCM-Fusion. RCM-Fusion uses each backbone network to obtain the radar features and camera features. The multi-modal features are then fused in the Radar Guided BEV Encoder module for feature-level fusion. For instance-level fusion, the Radar Grid Point Refinement module refines the initial results with a novel grid feature pooling method.

preprocessed radar points represented by 3D coordinates (x, y, z) , RCS, and Doppler velocity (v_x, v_y) are encoded by the pillar encoding module and passed through the pillar scatter followed by 2D CNN module to obtain the radar BEV feature map $F_R \in \mathbb{R}^{H \times W \times C}$. The detailed architecture of the radar backbone network can be found in Appendix A.1.

3.2. Radar Guided BEV Encoder

The Radar Guided BEV Encoder utilizes F_R and F_C as inputs to generate enhanced BEV features. First, we use F_R to create a Radar Guided BEV Query (RGBQ) containing positional information from the radar. Then, we use the RGBQs to transform multi-modal features into individual enhanced BEV features. Finally, the Radar-Camera Gating (RCG) performs the gated aggregation of two BEV features taking into account the difference in the amount of information between the two BEV features.

Radar Guided BEV Query. In order to achieve feature-level fusion of the radar and camera data, we need to transform F_C to a BEV representation. Our baseline model, BEVFormer [16], leverages the BEV query concept and transformer-based structure to perform view transformation. To boost the accuracy of this view transformation further, depth information in radar data can be utilized. Towards this goal, we use the positional information provided by the radar BEV feature map F_R to obtain an enhanced BEV query termed the Radar Guided BEV query $Q^{RG} \in \mathbb{R}^{H \times W \times C}$. This Radar Guided BEV query serves to transform F_C and F_R into the enhanced BEV representations, respectively. Specifically, Q^{RG} is generated by

concatenating F_R with BEV queries $Q \in \mathbb{R}^{H \times W \times C}$ and passing it through a deformable self-attention (DeformAttn) module [49] as

$$Q_p^{RG} = \sum_{V \in \{Q, F_R\}} \text{DeformAttn}(Q_p, p, V), \quad (1)$$

where Q_p^{RG} and Q_p indicate the queries located at BEV plane pixel $p = (x, y)$. Then, Q_p^{RG} is used to decode the camera and radar features through spatial-cross attention (SCA) block [16], generating the refined camera BEV features B_C and the refined radar BEV features B_R as Eq. (2) and Eq. (3)

$$B_C = \text{SCA}_C(Q_p^{RG}, F_C) \quad (2)$$

$$B_R = \text{SCA}_R(Q_p^{RG}, F_R), \quad (3)$$

where SCA block is an operation that projects Q_p^{RG} to each sensor feature and then performs deformable cross-attention [49].

Radar-Camera Gating. Two refined BEV feature maps B_R and B_C are fused by their weighted combination

$$B_{RC} = \{\sigma(\text{Conv}_C[B_C; B_R]) \odot B_C\} \oplus \{\sigma(\text{Conv}_R[B_R; B_C]) \odot B_R\}, \quad (4)$$

where B_{RC} denotes the fused BEV feature map, $\sigma(\cdot)$ denotes a sigmoid function, \odot , \oplus and $[\cdot]$ denote the element-wise multiplication, element-wise summation, and channel-wise concatenation, respectively. Conv_C and Conv_R are convolutional layers for camera and radar, respectively. The

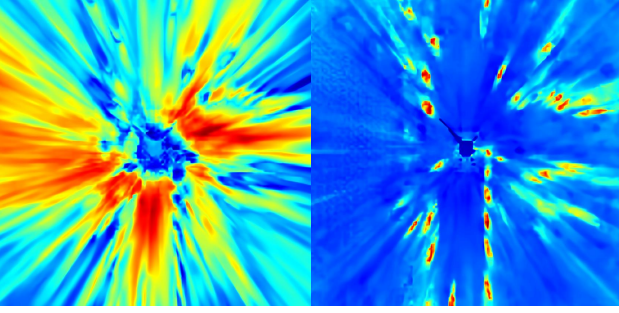


Figure 3. Visualization of the BEV feature map. Left: BEV feature map from BEVFormer-S [16], a single-frame version of BEVFormer. Right: BEV feature map obtained from Radar Guided BEV Encoder. Compared to the left figure, the right figure shows that the positional information provided by the radar BEV feature map allows the features to better localize the regions where objects exist.

gating operation adaptively weights the radar and camera BEV feature maps taking into account information from both sides. This gating operation is implemented using a sigmoid function followed by convolutional layers. Next, the fused BEV feature map B_{RC} is passed through normalization and feed-forward network in the same manner as our baseline models, and the final BEV feature map is produced by repeating the BEV encoder section L times. When using the Radar Guided BEV Encoder module, a more sophisticated feature map can be created based on radar positional information, compared to the existing camera-only method. As seen in Figure 3, our baseline model, BEVFormer-S [16], has an imprecise BEV feature map due to inadequate depth information. In contrast, the enhanced feature map generated by the Radar Guided BEV Encoder concentrates near the Ground Truth (GT) bounding box. Please refer to Appendix A.2 for the detailed structure.

3.3. Radar Grid Point Refinement

In this section, we propose a novel instance-level fusion based on the Radar Grid Point Refinement module. The Proposal-aware Radar Attention (PRA) takes 3D proposals and their associated radar points as input and utilizes MLP-based attention layers to determine the importance of each radar point. Then, Radar Grid Point Pooling (RGPP) considers the characteristics and distribution of radar points to sample the grid points, and then integrates the radar point features and multi-scale image features into the grid points to generate refined features. Finally, the refined features and the initial proposal features are combined to produce the final output.

Proposal-aware Radar Attention. We used the Soft Polar Association (SPA) method implemented in CRAFT [11] to associate the radar points with 3D proposals. The SPA method transforms 3D proposals and radar points into po-

lar coordinates, and assigns the radar points within a fixed range in both azimuth and radial directions to the 3D proposal. However, as more radar points are assigned to a larger area around a 3D proposal, some of them may not be relevant to the proposal. PRA module can be used to solve these problems. Let b denote one of the N proposals found by the first stage detection, where $b = (\mathbf{c}, w, l, h, \theta, \mathbf{v}_{pred})$ consist of 3D proposal center location \mathbf{c} , 3D dimension (w, l, h) , orientation θ and velocity \mathbf{v}_{pred} . The K radar points associated with b are denoted by $\{r_k\}_{k=1}^K$, and the 3D position of the k th point r_k is $\mathbf{u}_k \in \mathbb{R}^3$. Encoding the radar point features and relative positions between \mathbf{c} and \mathbf{u}_k , we calculate a point-wise score vector s_k to determine the importance of the points and obtain the attended radar point features a_k as

$$s_k = \text{MLP}_2([\text{MLP}_1(r_k); \delta(\mathbf{c} - \mathbf{u}_k)]) \quad (5)$$

$$a_k = \text{softmax}(s_k) \odot \text{MLP}_3(r_k), \quad (6)$$

where $\text{MLP}(\cdot)$ denotes the channel-wise MLPs, $\delta(\cdot)$ denotes the positional encoding and $\text{softmax}(\cdot)$ denotes the Softmax function.

Radar Grid Point Pooling. The positioning and quantity of grid points have the most significant impact on the efficacy of the grid point-based refinement module [4, 23, 30]. In particular, radar points have a very low point density and a high positional error compared to LiDAR, which makes the grid point sampling more critical. Therefore, we propose the RGPP module, an adaptive grid point pooling technique that takes into account the characteristics of radar points. As shown in Fig. 4, the velocity vector \mathbf{v}_{pred} of 3D proposals, can be decomposed as the tangential velocity \mathbf{v}_{tan} and the radial velocity \mathbf{v}_{rad} . For the k^{th} radar point r_k , T grid points $\{g_k^t\}_{t=0}^{T-1}$ are generated around the radar point’s position \mathbf{u}_k according to

$$\gamma = \begin{cases} \rho_{min}, & |\mathbf{v}_{tan}| \leq \rho_{min} \\ |\mathbf{v}_{tan}|, & \rho_{min} < |\mathbf{v}_{tan}| < \rho_{max} \\ \rho_{max}, & |\mathbf{v}_{tan}| \geq \rho_{max} \end{cases} \quad (7)$$

$$g_k^t = \gamma \cdot \left(\frac{t}{T-1} - \frac{1}{2} \right) \cdot \frac{\mathbf{v}_{tan} |\mathbf{v}_{tan}|}{|\mathbf{v}_{tan}|} \mathbf{u}_k, t = 0, \dots, T-1. \quad (8)$$

We create the grid points in the direction of \mathbf{v}_{tan} . This arrangement is because radar points tend to be noisier in the tangential direction, so the grid points need to be widely distributed in this direction to capture a variety of radar point features. The range of the grid points is determined by γ , which is proportional to the magnitude of \mathbf{v}_{tan} . Since \mathbf{v}_{tan} have predicted values, it may not be accurate, and grid points may not be generated correctly. Therefore, we set the upper bound ρ_{max} and the lower bound ρ_{min} for the range γ . For each 3D proposal, KT grid points are generated from

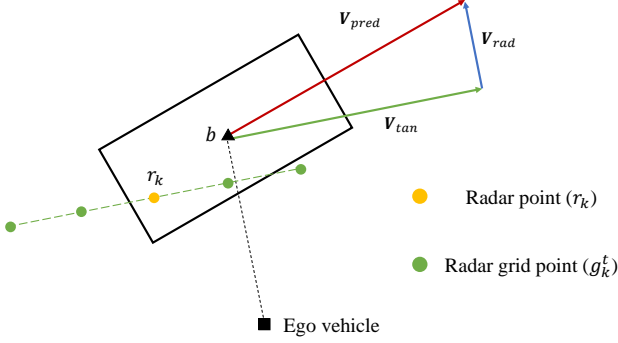


Figure 4. Illustration of novel adaptive grid point sampling. For each radar point associated with the proposal, T grid points are generated in a tangential direction.

all radar points assigned to it, and then Farthest Point Sampling (FPS) is utilized to select M grid points $\{g_m\}_{m=1}^M$ to maintain a fixed number of grid points.

Next, we use the grid points $\{g_m\}_{m=1}^M$ as a basis for extracting radar point features and image features and generating the fused grid features. First, the set abstraction (SetAbs) [30] encodes the radar points around each grid point g_m to produce the radar point features F_m^{pts}

$$F_m^{pts} = \text{SetAbs}(\{a_k\}_{k=1}^K, \{r_k\}_{k=1}^K, g_m). \quad (9)$$

In parallel, the grid points are projected onto F_C in the camera view and then the camera features F_m^{img} are obtained through a bilinear interpolation

$$F_m^{img} = \text{Bilinear}(F_C, \text{proj}(g_m)), \quad (10)$$

where $\text{proj}(\cdot)$ denotes the projection to the camera view. Finally, the proposal features F_m^{obj} are obtained by fusing F_m^{pts} and F_m^{img}

$$F_m^{obj} = \text{maxpool}(F_m^{pts} \oplus F_m^{img}), \quad (11)$$

and these features are fused with the initial proposal features to perform 3D proposal refinement.

3.4. Radar Data Preprocessing

In order to effectively use radars, it is essential to comprehend their characteristics. Radar point clouds have the advantage of providing additional information such as RCS and Doppler velocity, but have a limited resolution compared to LiDAR due to the small number of points. According to the nuScenes dataset [1], a LiDAR sensor can obtain up to 20,000 data points in a single scan, while a total of five radar sensors provide only approximately 430 points. However, only about 200 points were deemed valid based on cluster validity, dynamic properties, and Doppler ambiguity status. We reduced the strictness of the cluster validity and ambiguity filters to maximize the efficiency of the

deep learning model, resulting in an increase of the number of points to 380. Additionally, the multi-sweep integrator used in the existing LiDAR-only method was altered to conform to the radar characteristics, thus significantly increasing the radar point density. In the case of LiDAR-based multi-sweep integrators, it is possible to compensate for the ego vehicle’s movement, however, the movement of the individual points cannot be rectified due to the absence of velocity information. On the other hand, radial velocity values can be utilized to compensate for the movement of radar points against those acquired from other sweeps. This allows for an enhanced accumulation of points. By employing this method, approximately 2200 radar points are accepted as model input per sample.

4. Experiments

In this section, we evaluate the performance of the proposed RCM-Fusion on the nuScenes dataset.

4.1. Datasets

We verified the performance of our model using nuScenes [1] dataset, a representative open data set for autonomous driving. According to the official division, the nuScenes dataset consists of 700, 150, and 150 scenes for training, validation, and testing, respectively. The nuScenes dataset evaluates 3D object detection performance using mean Average Precision (mAP) and the nuScenes Detection score (NDS). The mAP is calculated based on the BEV center distance between the ground truth and the predicted results, and the final mAP is computed by averaging over distance thresholds of 0.5, 1, 2, and 4 meters. True Positive (TP) is defined as a prediction box within 2 meters of the ground-truth box, and the five TP metrics used for evaluation include translation, scale, orientation, velocity, and attribute errors. Finally, the overall object detection performance is measured using the NDS which takes into account both mAP and the five TP metrics.

4.2. Implementation Details

For our baseline model, we use a static version of BEVFormer [16], or BEVFormer-S that only utilizes single-frame data. For the camera backbone, we use pre-trained weights of FCOS3D [34] and process the image size to 900×1600 . For the radar backbone, we do not use pre-trained weights and train the entire model in an end-to-end fashion without weight freezing. We use the AdamW [21] optimizer with a learning rate of $2e-4$ and train a total of 24 epochs, employing the class balancing strategy, CBGS proposed in [48]. All ablation studies use 1/7 of the nuScenes training dataset and apply the CBGS technique. Please refer to Appendix B.1 for more details.

Methods	Input	NDS \uparrow	mAP \uparrow	mATE \downarrow	mASE \downarrow	mAOE \downarrow	mAVE \downarrow	mAAE \downarrow
PointPillars [12]	L	45.3	30.5	0.517	0.290	0.500	0.316	0.368
FCOS3D [34]	C	42.8	35.8	0.690	0.249	0.452	1.434	0.124
PGD [33]	C	44.8	38.6	0.626	0.245	0.451	1.509	0.127
DD3D* [25]	C	47.7	41.8	0.572	0.249	0.368	1.014	0.124
DETR3D* [36]	C	47.9	41.2	0.641	0.255	0.394	0.845	0.133
BEVDet* [7]	C	48.8	42.4	0.524	0.242	0.373	0.950	0.148
PETR [19]	C	45.5	39.1	0.647	0.251	0.433	0.933	0.143
Graph-DETR3D [3]	C	47.2	41.8	0.668	0.250	0.440	0.876	0.139
Ego3RT [22]	C	44.3	38.9	0.599	0.268	0.470	1.169	0.172
BEVFormer-S [16]	C	46.2	40.9	0.650	0.261	0.439	0.925	0.147
PolarFormer [9]	C	47.0	41.5	0.657	0.263	0.405	0.911	0.139
M ² BEV [37]	C	47.4	42.9	0.583	0.254	0.376	1.053	0.190
CenterFusion [24]	C+R	44.9	32.6	0.631	0.261	0.516	0.614	0.115
CRAFT [11]	C+R	52.3	41.1	0.467	0.268	0.456	0.519	0.114
RCM-Fusion (Ours)	C+R	58.0	49.3	0.485	0.255	0.386	0.421	0.115

Table 1. Performance comparisons on the nuScenes test set. ‘L’, ‘C’, and ‘R’ represent LiDAR, camera, and radar, respectively. * are trained with external data.

Stage 1		Stage 2		Performance	
w/ RGBQ	w/ RCG	w/ RGPP	w/ PRA	NDS \uparrow	mAP \uparrow
				44.9	37.9
✓				52.5	42.2
✓	✓			53.1	42.9
✓	✓	✓		53.4	43.1
✓	✓	✓	✓	53.7	43.5

Table 2. Component analysis on the nuScenes validation set. RGBQ: the Radar Guided BEV Query. RCG: the Radar-Camera Gating. RGPP: the Radar Grid Point Pooling. PRA: the Proposal-aware Radar Attention.

4.3. Data Augmentation

Recently, BEVDet [7] proposed both image data augmentation (IDA) and BEV data augmentation (BDA) for training camera-only object detectors. We applied these methods to RCM-Fusion. This was achieved by associating the radar points with camera pixels using a camera-to-3D coordinate transformation. Also, we adopted the cross-modal GT-AUG approach typically used for LiDAR-camera fusion models [2, 32, 46] to RCM-Fusion. Radar usually has far fewer points within the ground truth than LiDAR, and it is not uncommon for some GT boxes to have no radar points at all. To address this, we applied an existing method to polar coordinates to boost the number of non-empty GT boxes. For more details about data augmentation, please refer to Appendix B.2.

Methods	NDS \uparrow	mAP \uparrow
w/o Grid Points	53.3	43.0
Regular Grid Points	53.2	43.0
Adaptive Grid Points	53.7	43.5

Table 3. Ablation studies of grid point sampling. w/o Grid Points refers to the method of substituting radar points with grid points. Regular Grid Points refers to a method that generates a fixed number of grid points [30].

4.4. Results on the nuScenes Dataset

We compare our RCM-Fusion with state-of-the-art camera-based and radar-camera fusion detectors trained with a single frame on the nuScenes test set. According to Table 1, our RCM-Fusion exhibits superior performances in terms of mAP and NDS metrics compared to the previous camera-based models and radar-camera fusion models. Compared to CRAFT [11], the best performer among the existing radar-camera fusion models, RCM-Fusion outperforms by 8.2% in mAP and 5.7% in NDS. Compared with our baseline model, BEVFormer-S [16], RCM-Fusion achieves 11.8% and 8.4% performance gains in NDS and mAP, respectively.

4.5. Ablation Studies on the nuScenes Valid Set

Component Analysis. The contributions of Radar Guided BEV Query (RGBQ), Radar-Camera Gating (RCG), Proposal-aware Radar Attention (PRA) and Radar Grid Point Pooling (RGPP) to the overall performance are presented in Table 2. Using radar pillar features to enhance

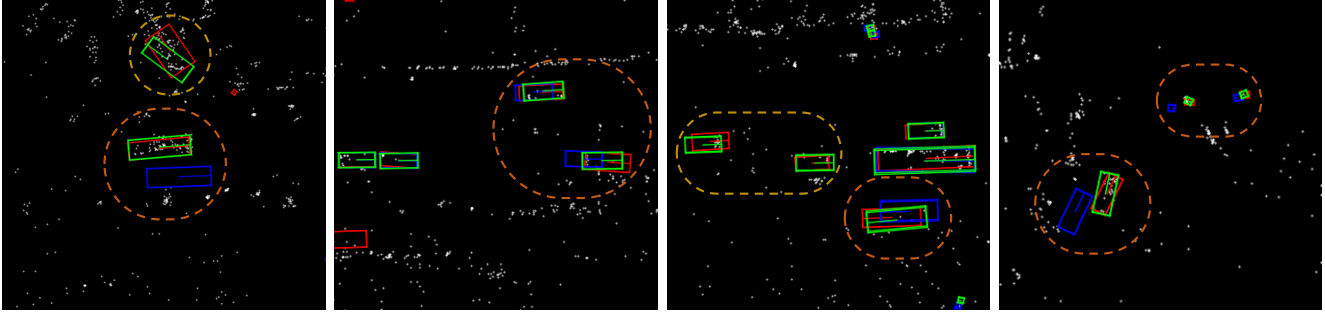


Figure 5. We visualized the predictions of RCM-Fusion (green boxes) and camera-only baseline model, BEVFormer-S (blue boxes), alongside the GT (red boxes) on a bird’s eye view. The figures demonstrate that the RCM-Fusion predicts more accurate results (in the orange regions), and it is able to detect what the camera-only baseline fails to identify (in the yellow regions).

Data Augmentation Methods			Performance	
IDA + BDA	GT-AUG	PGT-AUG	NDS↑	mAP↑
			51.4	42.1
✓			53.1	43.3
✓	✓		52.3	42.7
✓		✓	53.7	43.5

Table 4. Ablation studies of data augmentation. IDA: Image Data Augmentation. BDA: BEV Data Augmentation. GT-AUG: Standard GT sampling strategy. PGT-AUG: GT sampling strategy in polar coordinate.

the BEV query, RGBQ improved 4.3% in mAP and 7.6% in NDS compared to the baseline. RCG that adaptively fuses multi-modal BEV features additionally achieves performance gains of 0.7% in mAP and 0.6% in NDS. In the instance-level fusion, RGPP, which fuses the multi-modal features based on the adaptive grid points, further improves the performance by 0.2% in mAP and 0.3% in NDS. Finally, adding the RPA module leads to a 0.3% performance gain in mAP and 0.4% in NDS compared to the baseline.

Qualitative Results. In Fig. 5, the detection results from RCM-Fusion were visualized for various scenarios. By capitalizing on the position data provided by the radar, RCM-Fusion localizes the objects more accurately than the camera-only baseline model, BEVFormer-S. Furthermore, our model can identify the existence of objects that are not well detected by the camera-only baseline model.

Effects of Radar Grid Point Sampling. We investigate the effectiveness of the proposed grid point generation method. Table 3 compares the proposed method with other methods. The w/o Grid Points (w/o GP) is a method that does not generate grid points and directly uses the radar points associated with the proposal for refinement. The Regular Grid Point (RGP) method generates a fixed number of grid points, similar to [30]. RGP is effective for a two-stage 3D detector using LiDAR, but since the radar points are very sparse, there may not be any radar points around the grid points. Consequently, it is analyzed that the RGP has a sim-

Radar Filtering Method		# pts	Performance	
Cluster validity	Doppler ambiguity		NDS↑	mAP↑
Valid	Unambiguous	200	53.0	43.1
Valid States	Unambiguous	367	52.8	42.7
Valid States	Valid States	380	53.7	43.5
All Points	All Points	433	52.9	43.0

Table 5. Ablation studies of radar point filtering methods. ‘# pts’ denotes the number of average points per sweep.

ilar performance to the w/o GP method due to the lack of useful grid points being useful for refinement. However, by applying Adaptive Grid Points, only useful grid points can be generated, thus enabling an effective refinement.

Data Augmentation. The effects of the data augmentation strategies, IDA, BDA, GT Aug and PGT Aug were evaluated in Table. 4. The IDA and BDA methods improve mAP by 1.2% and NDS by 1.7% compared to the model without augmentation. Furthermore, though the typical GT-AUG approach shows a decrease in performance, the proposed PGT-AUG increases the mAP by 0.2% and the NDS by 0.6%.

Radar Data Filtering. Table. 5 demonstrates that our radar point filtering method is effective. Without applying filters (fourth row), the number of noisy radar points increases but it results in worse performance than the default setting (first row). However, by applying appropriate filtering (third row), the increase in radar points offers the performance gain of 1.1% in NDS and 0.5% in mAP over the first row.

5. Conclusions

In this paper, we proposed a novel radar-camera 3D detector, RCM-Fusion. RCM-Fusion fused the radar and camera data at both the feature-level and instance-level for enhanced 3D object detection. We demonstrated that the Radar Guided BEV Encoder could achieve effective transformation of camera features into BEV, leveraging the radar features. Moreover, the Radar Grid Point Refinement pro-

posed a novel grid pooling technique, which fused both radar and camera features based on the adaptive point grids to refine the initial 3D proposals. For future work, we plan to extend our method to a time-efficient multi-frame radar-camera fusion method.

References

- [1] Holger Caesar, Varun Bankiti, Alex H Lang, Sourabh Vora, Venice Erin Liong, Qiang Xu, Anush Krishnan, Yu Pan, Giancarlo Baldan, and Oscar Beijbom. nuscenes: A multi-modal dataset for autonomous driving. In *Proceedings of the IEEE/CVF Conference on Computer Vision and Pattern Recognition*, pages 11621–11631, 2020.
- [2] Zehui Chen, Zhenyu Li, Shiquan Zhang, Liangji Fang, Qin-hong Jiang, and Feng Zhao. Autoalignv2: Deformable feature aggregation for dynamic multi-modal 3d object detection. *arXiv preprint arXiv:2207.10316*, 2022.
- [3] Zehui Chen, Zhenyu Li, Shiquan Zhang, Liangji Fang, Qin-hong Jiang, and Feng Zhao. Graph-detr3d: rethinking overlapping regions for multi-view 3d object detection. In *Proceedings of the 30th ACM International Conference on Multimedia*, pages 5999–6008, 2022.
- [4] Jiajun Deng, Shaoshuai Shi, Peiwei Li, Wengang Zhou, Yanyong Zhang, and Houqiang Li. Voxel r-cnn: Towards high performance voxel-based 3d object detection. *arXiv preprint arXiv:2012.15712*, 1(2):4, 2020.
- [5] Kaiming He, Xiangyu Zhang, Shaoqing Ren, and Jian Sun. Deep residual learning for image recognition. In *Proceedings of the IEEE/CVF Conference on Computer Vision and Pattern Recognition*, pages 770–778, 2016.
- [6] Junjie Huang and Guan Huang. Bevdet4d: Exploit temporal cues in multi-camera 3d object detection. *arXiv preprint arXiv:2203.17054*, 2022.
- [7] Junjie Huang, Guan Huang, Zheng Zhu, and Dalong Du. Bevdet: High-performance multi-camera 3d object detection in bird-eye-view. *arXiv preprint arXiv:2112.11790*, 2021.
- [8] Jyh-Jing Hwang, Henrik Kretzschmar, Joshua Manela, Sean Rafferty, Nicholas Armstrong-Crews, Tiffany Chen, and Dragomir Anguelov. Cramnet: Camera-radar fusion with ray-constrained cross-attention for robust 3d object detection. In *Computer Vision–ECCV 2022: 17th European Conference, Tel Aviv, Israel, October 23–27, 2022, Proceedings, Part XXXVIII*, pages 388–405. Springer, 2022.
- [9] Yanqin Jiang, Li Zhang, Zhenwei Miao, Xiatian Zhu, Jin Gao, Weiming Hu, and Yu-Gang Jiang. Polarformer: Multi-camera 3d object detection with polar transformers. *arXiv preprint arXiv:2206.15398*, 2022.
- [10] Youngseok Kim, Jun Won Choi, and Dongsuk Kum. Grif net: Gated region of interest fusion network for robust 3d object detection from radar point cloud and monocular image. In *2020 IEEE/RSJ International Conference on Intelligent Robots and Systems (IROS)*, pages 10857–10864. IEEE, 2020.
- [11] Youngseok Kim, Sanmin Kim, Jun Won Choi, and Dongsuk Kum. Craft: Camera-radar 3d object detection with spatio-contextual fusion transformer. In *Proceedings of the AAAI Conference on Artificial Intelligence*, 2023.
- [12] Alex H Lang, Sourabh Vora, Holger Caesar, Lubing Zhou, Jiong Yang, and Oscar Beijbom. Pointpillars: Fast encoders for object detection from point clouds. In *Proceedings of the IEEE/CVF Conference on Computer Vision and Pattern Recognition*, pages 12697–12705, 2019.
- [13] Yinhao Li, Zheng Ge, Guanyi Yu, Jinrong Yang, Zengran Wang, Yukang Shi, Jianjian Sun, and Zeming Li. Bevdepth: Acquisition of reliable depth for multi-view 3d object detection. *arXiv preprint arXiv:2206.10092*, 2022.
- [14] Yu-Jhe Li, Jinhyung Park, Matthew O’Toole, and Kris Kitani. Modality-agnostic learning for radar-lidar fusion in vehicle detection. In *Proceedings of the IEEE/CVF Conference on Computer Vision and Pattern Recognition*, pages 918–927, 2022.
- [15] Zhichao Li, Feng Wang, and Naiyan Wang. Lidar r-cnn: An efficient and universal 3d object detector. In *Proceedings of the IEEE/CVF Conference on Computer Vision and Pattern Recognition*, pages 7546–7555, 2021.
- [16] Zhiqi Li, Wenhai Wang, Hongyang Li, Enze Xie, Chonghao Sima, Tong Lu, Yu Qiao, and Jifeng Dai. Bevformer: Learning bird’s-eye-view representation from multi-camera images via spatiotemporal transformers. In *Computer Vision–ECCV 2022: 17th European Conference, Tel Aviv, Israel, October 23–27, 2022, Proceedings, Part IX*, pages 1–18. Springer, 2022.
- [17] Teck-Yian Lim, Amin Ansari, Bence Major, Daniel Fontijne, Michael Hamilton, Radhika Gowaikar, and Sundar Subramanian. Radar and camera early fusion for vehicle detection in advanced driver assistance systems. In *Machine learning for autonomous driving workshop at the 33rd conference on neural information processing systems*, volume 2, page 7, 2019.
- [18] Tsung-Yi Lin, Piotr Dollár, Ross Girshick, Kaiming He, Bharath Hariharan, and Serge Belongie. Feature pyramid networks for object detection. In *Proceedings of the IEEE/CVF Conference on Computer Vision and Pattern Recognition*, pages 2117–2125, 2017.
- [19] Yingfei Liu, Tiancai Wang, Xiangyu Zhang, and Jian Sun. Petr: Position embedding transformation for multi-view 3d object detection. In *Computer Vision–ECCV 2022: 17th European Conference, Tel Aviv, Israel, October 23–27, 2022, Proceedings, Part XXVII*, pages 531–548. Springer, 2022.
- [20] Yunfei Long, Abhinav Kumar, Daniel Morris, Xiaoming Liu, Marcos Castro, and Punarjay Chakravarty. Radiant: Radar-image association network for 3d object detection. *arXiv preprint arXiv:2206.15398*, 2023.
- [21] Ilya Loshchilov and Frank Hutter. Decoupled weight decay regularization. *arXiv preprint arXiv:1711.05101*, 2017.
- [22] Jiachen Lu, Zheyuan Zhou, Xiatian Zhu, Hang Xu, and Li Zhang. Learning ego 3d representation as ray tracing. In *Computer Vision–ECCV 2022: 17th European Conference, Tel Aviv, Israel, October 23–27, 2022, Proceedings, Part XXVI*, pages 129–144. Springer, 2022.
- [23] Jiageng Mao, Minzhe Niu, Haoyue Bai, Xiaodan Liang, Hang Xu, and Chunjing Xu. Pyramid r-cnn: Towards better performance and adaptability for 3d object detection. In *Proceedings of the IEEE/CVF International Conference on Computer Vision*, pages 2723–2732, 2021.
- [24] Ramin Nabati and Hairong Qi. Centerfusion: Center-based radar and camera fusion for 3d object detection. In *Proceed-*

- ings of the *IEEE/CVF Winter Conference on Applications of Computer Vision*, pages 1527–1536, 2021.
- [25] Dennis Park, Rares Ambrus, Vitor Guizilini, Jie Li, and Adrien Gaidon. Is pseudo-lidar needed for monocular 3d object detection? In *Proceedings of the IEEE/CVF International Conference on Computer Vision*, pages 3142–3152, 2021.
- [26] Charles R Qi, Hao Su, Kaichun Mo, and Leonidas J Guibas. Pointnet: Deep learning on point sets for 3d classification and segmentation. In *Proceedings of the IEEE/CVF Conference on Computer Vision and Pattern Recognition*, pages 652–660, 2017.
- [27] Charles Ruizhongtai Qi, Li Yi, Hao Su, and Leonidas J Guibas. Pointnet++: Deep hierarchical feature learning on point sets in a metric space. *Advances in neural information processing systems*, 30, 2017.
- [28] Kun Qian, Shilin Zhu, Xinyu Zhang, and Li Erran Li. Robust multimodal vehicle detection in foggy weather using complementary lidar and radar signals. In *Proceedings of the IEEE/CVF Conference on Computer Vision and Pattern Recognition*, pages 444–453, 2021.
- [29] Hualian Sheng, Sijia Cai, Yuan Liu, Bing Deng, Jianqiang Huang, Xian-Sheng Hua, and Min-Jian Zhao. Improving 3d object detection with channel-wise transformer. In *Proceedings of the IEEE/CVF International Conference on Computer Vision*, pages 2743–2752, 2021.
- [30] Shaoshuai Shi, Chaoxu Guo, Li Jiang, Zhe Wang, Jianping Shi, Xiaogang Wang, and Hongsheng Li. Pv-rnn: Point-voxel feature set abstraction for 3d object detection. In *Proceedings of the IEEE/CVF Conference on Computer Vision and Pattern Recognition*, pages 10529–10538, 2020.
- [31] Shaoshuai Shi, Xiaogang Wang, and Hongsheng Li. Pointcnn: 3d object proposal generation and detection from point cloud. In *Proceedings of the IEEE/CVF Conference on Computer Vision and Pattern Recognition*, pages 770–779, 2019.
- [32] Chunwei Wang, Chao Ma, Ming Zhu, and Xiaokang Yang. Pointaugmenting: Cross-modal augmentation for 3d object detection. In *Proceedings of the IEEE/CVF Conference on Computer Vision and Pattern Recognition*, pages 11794–11803, 2021.
- [33] Tai Wang, ZHU Xinge, Jiangmiao Pang, and Dahua Lin. Probabilistic and geometric depth: Detecting objects in perspective. In *Conference on Robot Learning*, pages 1475–1485. PMLR, 2022.
- [34] Tai Wang, Xinge Zhu, Jiangmiao Pang, and Dahua Lin. Fcos3d: Fully convolutional one-stage monocular 3d object detection. In *Proceedings of the IEEE/CVF International Conference on Computer Vision*, pages 913–922, 2021.
- [35] Yan Wang, Wei-Lun Chao, Divyansh Garg, Bharath Hariharan, Mark Campbell, and Kilian Q Weinberger. Pseudo-lidar from visual depth estimation: Bridging the gap in 3d object detection for autonomous driving. In *Proceedings of the IEEE/CVF Conference on Computer Vision and Pattern Recognition*, pages 8445–8453, 2019.
- [36] Yue Wang, Vitor Campagnolo Guizilini, Tianyuan Zhang, Yilun Wang, Hang Zhao, and Justin Solomon. Detr3d: 3d object detection from multi-view images via 3d-to-2d queries. In *Conference on Robot Learning*, pages 180–191. PMLR, 2022.
- [37] Enze Xie, Zhiding Yu, Daquan Zhou, Jonah Philion, Anima Anandkumar, Sanja Fidler, Ping Luo, and Jose M Alvarez. M²bev: Multi-camera joint 3d detection and segmentation with unified birds-eye view representation. *arXiv preprint arXiv:2204.05088*, 2022.
- [38] Yan Yan, Yuxing Mao, and Bo Li. Second: Sparsely embedded convolutional detection. *Sensors*, 18(10):3337, 2018.
- [39] Bin Yang, Runsheng Guo, Ming Liang, Sergio Casas, and Raquel Urtasun. Radarnet: Exploiting radar for robust perception of dynamic objects. In *Computer Vision—ECCV 2020: 16th European Conference, Glasgow, UK, August 23–28, 2020, Proceedings, Part XVIII 16*, pages 496–512. Springer, 2020.
- [40] Chenyu Yang, Yuntao Chen, Hao Tian, Chenxin Tao, Xizhou Zhu, Zhaoxiang Zhang, Gao Huang, Hongyang Li, Yu Qiao, Lewei Lu, et al. Bevformer v2: Adapting modern image backbones to bird’s-eye-view recognition via perspective supervision. *arXiv preprint arXiv:2211.10439*, 2022.
- [41] Honghui Yang, Zili Liu, Xiaopei Wu, Wenxiao Wang, Wei Qian, Xiaoqi He, and Deng Cai. Graph r-cnn: Towards accurate 3d object detection with semantic-decorated local graph. In *Computer Vision—ECCV 2022: 17th European Conference, Tel Aviv, Israel, October 23–27, 2022, Proceedings, Part VIII*, pages 662–679. Springer, 2022.
- [42] Zetong Yang, Yanan Sun, Shu Liu, and Jiaya Jia. 3dssd: Point-based 3d single stage object detector. In *Proceedings of the IEEE/CVF Conference on Computer Vision and Pattern Recognition*, pages 11040–11048, 2020.
- [43] Zetong Yang, Yanan Sun, Shu Liu, Xiaoyong Shen, and Jiaya Jia. Std: Sparse-to-dense 3d object detector for point cloud. In *Proceedings of the IEEE/CVF International Conference on Computer Vision*, pages 1951–1960, 2019.
- [44] Tianwei Yin, Xingyi Zhou, and Philipp Krahenbuhl. Center-based 3d object detection and tracking. In *Proceedings of the IEEE/CVF Conference on Computer Vision and Pattern Recognition*, pages 11784–11793, 2021.
- [45] Tianwei Yin, Xingyi Zhou, and Philipp Krahenbuhl. Center-based 3d object detection and tracking. In *Proceedings of the IEEE/CVF Conference on Computer Vision and Pattern Recognition*, pages 11784–11793, 2021.
- [46] Wenwei Zhang, Zhe Wang, and Chen Change Loy. Exploring data augmentation for multi-modality 3d object detection. *arXiv preprint arXiv:2012.12741*, 2020.
- [47] Yin Zhou and Oncel Tuzel. Voxelnet: End-to-end learning for point cloud based 3d object detection. In *Proceedings of the IEEE/CVF Conference on Computer Vision and Pattern Recognition*, pages 4490–4499, 2018.
- [48] Benjin Zhu, Zhengkai Jiang, Xiangxin Zhou, Zeming Li, and Gang Yu. Class-balanced grouping and sampling for point cloud 3d object detection. *arXiv preprint arXiv:1908.09492*, 2019.
- [49] Xizhou Zhu, Weijie Su, Lewei Lu, Bin Li, Xiaogang Wang, and Jifeng Dai. Deformable detr: Deformable transformers for end-to-end object detection. *arXiv preprint arXiv:2010.04159*, 2020.